

# **UCLA**

## **UCLA Previously Published Works**

### **Title**

Motion frozen 18F-FDG cardiac PET

### **Permalink**

<https://escholarship.org/uc/item/6fj7t0fq>

### **Journal**

Journal of Nuclear Cardiology, 18(2)

### **ISSN**

1071-3581

### **Authors**

Le Meunier, Ludovic  
Slomka, Piotr J  
Dey, Damini  
et al.

### **Publication Date**

2011-04-01

### **DOI**

10.1007/s12350-010-9322-3

Peer reviewed

# ORIGINAL ARTICLE

## Motion frozen $^{18}\text{F}$ -FDG cardiac PET

Ludovic Le Meunier, PhD,<sup>a,c</sup> Piotr J. Slomka, PhD,<sup>a,b</sup> Damini Dey, PhD,<sup>a,b</sup> Amit Ramesh, MSc,<sup>b</sup> Louis E. J. Thomson, MBChB, FRACP,<sup>a</sup> Sean W. Hayes, MD,<sup>a</sup> John D. Friedman, MD,<sup>a</sup> Victor Cheng, MD,<sup>a</sup> Guido Germano, PhD,<sup>a,b</sup> and Daniel S. Berman, MD<sup>a,b</sup>

**Background.** PET reconstruction incorporating spatially variant 3D Point Spread Function (PSF) improves contrast and image resolution. “Cardiac Motion Frozen” (CMF) processing eliminates the influence of cardiac motion in static summed images. We have evaluated the combined use of CMF- and PSF-based reconstruction for high-resolution cardiac PET.

**Methods.** Static and 16-bin ECG-gated images of 20 patients referred for  $^{18}\text{F}$ -FDG myocardial viability scans were obtained on a Siemens Biograph-64. CMF was applied to the gated images reconstructed with PSF. Myocardium to blood contrast, maximum left ventricle (LV) counts to defect contrast, contrast-to-noise (CNR) and wall thickness with standard reconstruction (2D-AWSEM), PSF, ED-gated PSF, and CMF-PSF were compared.

**Results.** The measured wall thickness was  $18.9 \pm 5.2$  mm for 2D-AWSEM,  $16.6 \pm 4.5$  mm for PSF, and  $13.8 \pm 3.9$  mm for CMF-PSF reconstructed images (all  $P < .05$ ). The CMF-PSF myocardium to blood and maximum LV counts to defect contrasts ( $5.7 \pm 2.7$ ,  $10.0 \pm 5.7$ ) were higher than for 2D-AWSEM ( $3.5 \pm 1.4$ ,  $6.5 \pm 3.1$ ) and for PSF ( $3.9 \pm 1.7$ ,  $7.7 \pm 3.7$ ) (CMF vs all other,  $P < .05$ ). The CNR for CMF-PSF ( $26.3 \pm 17.5$ ) was comparable to PSF ( $29.1 \pm 18.3$ ), but higher than for ED-gated dataset ( $13.7 \pm 8.8$ ,  $P < .05$ ).

**Conclusion.** Combined CMF-PSF reconstruction increased myocardium to blood contrast, maximum LV counts to defect contrast and maintained equivalent noise when compared to static summed 2D-AWSEM and PSF reconstruction. (J Nucl Cardiol 2011;18:259–66.)

**Key Words:** Metabolism • PET • cardiac motion frozen • point spread function • cardiac imaging

### INTRODUCTION

The cardiac PET image quality can be limited by several factors including the intrinsic performance of the PET scanner. The distortions in the photon detection process due to the circular geometry of PET scanners and consequent increased tilting of the crystals off the center of the field of view (FOV) have a negative impact on the spatial resolution and on the noise in the reconstructed images. The recently introduced High-Definition Positron

Emission Tomography (HD-PET) technology (Siemens Healthcare Molecular Imaging, Knoxville, TN), reconstruction, significantly improves image spatial resolution and signal-to-noise ratio in the images using spatially variant detector spatial response with 3D-specific Point Spread Function (PSF) during the reconstruction step.<sup>1,2</sup> This type of resolution recovery reconstruction was introduced by other vendors as well and is termed in this manuscript as PSF reconstruction.

However, even with the improvements of PSF-based reconstruction in terms of spatial resolution and noise control, high-resolution myocardial imaging still faces the challenges of cardiac and respiratory motions, which degrade the static image quality by blurring the image. To address cardiac motion, the “Cardiac Motion Frozen” (CMF) technique has been developed previously by Slomka et al<sup>3</sup> for myocardial perfusion single-photon emission computed tomography (SPECT) images. This algorithm tracks the motion of the left ventricle (LV) in cardiac gated images, and then adjusts all cardiac phases to one phase (typically end diastolic) resulting in an image free of cardiac motion.

From the Departments of Imaging and Medicine,<sup>a</sup> Cedars-Sinai Medical Center, Los Angeles, CA; Department of Medicine,<sup>b</sup> David Geffen School of Medicine at UCLA, Los Angeles, CA; and Siemens Healthcare Molecular Imaging,<sup>c</sup> Knoxville, TN.

Received for publication Feb 23, 2010; final revision accepted Nov 20, 2010.

Reprint requests: Ludovic Le Meunier, PhD, Siemens Healthcare Molecular Imaging, 810 Innovation Dr, Knoxville, TN 37932; ludovic.lemeunier@siemens.com.

1071-3581/\$34.00

Copyright © 2010 The Author(s). This article is published with open access at Springerlink.com

doi:10.1007/s12350-010-9322-3

To our knowledge, CMF has never been evaluated in PET cardiac images. We hypothesized that CMF technique can further improve image quality of cardiac PET above that offered by resolution recovery as recently described.<sup>2</sup> In this study, the authors tested this hypothesis in cardiac PET with Fluorine-18 fluorodeoxyglucose (<sup>18</sup>F-FDG).<sup>4</sup> We describe the technique, and evaluate the improvement of CMF processing on image contrast, noise, myocardial wall thickness, and detectability of myocardial defects.

## MATERIALS AND METHODS

### PET Acquisition and Reconstruction

All images were acquired on a Siemens Biograph-64 TruePoint PET/CT with the TrueV option. This 3D system consists of a 64-slice CT and a PET scanner with 4 rings of Lutetium Oxyorthosilicate (LSO) detectors with a detector element dimensions of  $4 \times 4 \times 20$  mm<sup>3</sup>.<sup>5</sup> The image plane spacing is 2 mm. The PET axial and transaxial FOV are 216 and 605 mm respectively. The coincidence time window and the energy window are respectively 4.5 ns and 425-650 keV. The data was acquired in list mode format. A full description of the system performance can be found in.<sup>6</sup>

### Patient Acquisition

The authors retrospectively evaluated <sup>18</sup>F-FDG myocardial viability patient studies performed for clinical indications. Investigational Review Board (IRB) permission was obtained for retrospective analysis of this data. The overall study population consisted of 20 consecutive patients (16 males and 4 females) referred for myocardial viability assessment. Details about our patient cohort can be found in Table 1.

After at least 4 hours of fasting, 370 MBq of <sup>18</sup>F-FDG was injected intravenously to all patients. A 60-minute uptake

**Table 1.** Characteristics of the 20 patients included in this study

Characteristics	Mean $\pm$ SD	Range
Age (years)	62 $\pm$ 14	43-93
Weight (kg; lbs)	81 $\pm$ 13; 179 $\pm$ 29	63-107; 139-235
BMI (kg/m <sup>2</sup> )	28.5 $\pm$ 5.4	22.2-46.4
Diabetes	5/20	na
Prior MI	15/20	na
LV hypertrophy	12/20	na
EF	37 $\pm$ 12	21-59
Prevalence of MD	15/20	na
Extent of MD (%)	13.9 $\pm$ 15.8	0-47

BMI, Body Mass Index; MI, myocardial infarction; LV, left ventricle; MD, metabolic defect.

phase followed the injection. After a 2.8 second standard topogram acquisition (120 kVp), the patient underwent a CT scan for attenuation correction (CTAC) using the following parameters: spiral mode, slice thickness 3.0 mm, total scan time 3.36 s, pitch 1.5, rotation time 0.5 s, collimation 24  $\times$  1.2 mm, tube voltage 120 kVp, tube current 11 mAs. The estimated radiation dose for this CTAC acquisition was 0.3 mSv. Subsequently, <sup>18</sup>F-FDG emission data were acquired for 1 bed position around the heart (identical to the CT coverage of 210 mm). 3D PET ECG-gated 10-minute acquisition was performed in list mode. During both the CT and the PET acquisitions, the patients were instructed to breathe normally.

### Reconstruction Protocols

After sorting of the list file, static summed images were reconstructed with the standard reconstruction technique routinely used at our institution, 2D-Attenuation Weighted Ordered Subsets Expectation Maximization (AWOSEM) (3 iterations and 8 subsets), and with PSF (4 iterations and 14 subsets).<sup>2,7</sup> The number of iterations for the 2 reconstruction methods varies because of the difference in convergence speed between 2D-AWOSEM and PSF-based reconstruction. All the reconstruction parameters were optimized based on a phantom study in a previous work by our group.<sup>2</sup> 16-bin ECG-gated images were generated for PSF. Since the optimal spatial resolution with HD-PET was previously established in the air as 2 mm,<sup>1</sup> the authors chose to filter all patient images with a 2 mm Gaussian Filter (GF). The reconstruction matrix was 168  $\times$  168  $\times$  109 with a zoom of 2 and the pixel size was 2  $\times$  2  $\times$  2 mm<sup>3</sup>. Scatter correction, decay correction, and random correction were applied to the reconstructed images. CT-based attenuation correction was employed. When a misalignment was identified, a manual registration matrix with 3D-translations was generated by an experienced technologist and applied before the final reconstruction process. Both the original CT-PET alignment and the alignment after manual registration were checked by an expert imaging physician. Manual registration between PET and CT was applied before reconstruction. Manual CT-PET registration was performed in 5 cases out of the 20.

### Cardiac Motion Frozen Principle

CMF processing tracks the motion of the LV in cardiac gated images and then adjusts all cardiac phases to one phase (typically at end-diastole (ED)) resulting in an image free of cardiac motion. "Motion-freezing" is accomplished by motion tracking of the LV endo- and epicardial borders (Figure 1). The algorithm generates displacement vectors between each cardiac phase, and utilizes those vectors to put all the gates in the ED phase (Figure 1). The result is an image free of cardiac motion blurring (i.e., with the same spatial resolution of a single cardiac phase image), but with higher counting statistics and noise similar to static summed images. This algorithm has been previously described in details and validated for SPECT versus invasive angiography in.<sup>3</sup>

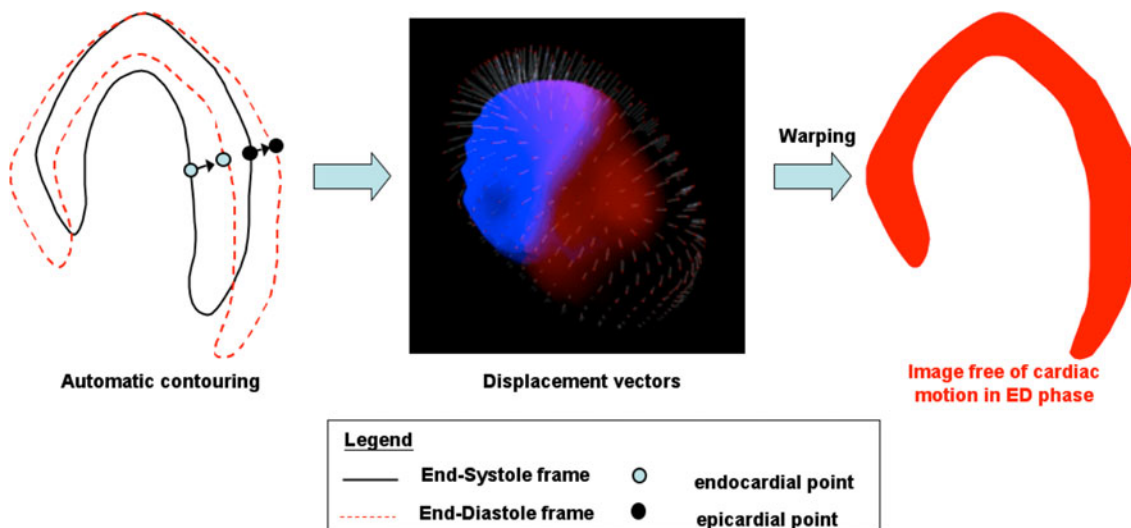


**Figure 1.** Diagram illustrating the principle of Cardiac Motion Frozen technique. (*Left*) Motion tracking of the left ventricle using selected points on endo- and epicardial surfaces. (*Middle*) Displacement vectors are generated between each cardiac phase. (*Right*) Starting from those vectors and using a warping technique, all the counts are put back in the end-diastole (ED) phase. The result is an image free of cardiac motion with the noise of a summed static image.

## Image Processing and Analysis

Short axis reorientation and automatic contouring of the LV in static and gated images were done automatically using QPET software (Cedars—Sinai Cardiac Package), for which input were transverse slices of reconstructed PET image.<sup>8</sup> CMF image processing technique was then applied to the gated datasets. The myocardial wall segment analysis was done with the 17-segment American Heart Association (AHA) model.<sup>9</sup>

**Myocardium to blood contrast and contrast-to-noise ratio.** Volumes of interest (VOI) over the LV and the blood pool (significantly larger than the spatial resolution in the image) were automatically derived based on the QPET segmentation of the LV. We calculated the contrast (Cont) between the blood pool and the myocardial wall, and the contrast-to-noise (CNR) as follows:

$$\text{Cont} = \frac{\text{mean(Ventricular\_VOI)}}{\text{mean(Blood\_VOI)}}$$

$$\text{CNR} = \frac{\text{mean(Ventricular\_VOI)} - \text{mean(Blood\_VOI)}}{\text{RMS}_\text{Noise}(\text{Blood\_VOI})},$$

where RMS\_Noise is the root mean square of the noise as defined by the standard deviation of the blood VOI. Contrast and CNR were calculated globally and for each of the 17 AHA-segments, from static summed images and CMF processed images.

**Contrast between defect and maximum uptake in myocardium (maximum LV counts to defect contrast).** The authors calculated the contrast between the average of the closest neighbors around the minimum (27 voxels) in segments with defects, and the average of the closest neighbors (27 voxels) around the maximum

of the myocardium. The segments with defects were identified using the original physician report based on standard 2D-AWOSEM images.

**Myocardial wall thickness.** Using the contours automatically detected by QPET, the authors estimated the wall thickness defined as the full width half maximum (FWHM) of a profile taken on the images at three different levels of the long axis (basal, mid, and apical) and with two orientations (septal to lateral and inferior to superior) for a total of 6 profiles per dataset.

## Statistical Analysis

All continuous variables are expressed as mean  $\pm$  one standard deviation. Paired *t* tests were used to compare differences in paired continuous data, and McNemar's tests were used to compare differences in paired discrete data. For unpaired continuous data, one-way ANOVA was used. All statistical tests were 2-tailed, and a value of  $P < .05$  was considered significant.

## RESULTS

### Myocardial Wall Thickness

The measured wall thickness was significantly smaller with CMF-PSF reconstruction as compared to 2D-AWOSEM and PSF reconstruction alone. We found that on average in 20 patients and over the 6 measured profiles, the wall thickness was  $18.9 \pm 5.2$  mm for 2D-AWOSEM,  $16.6 \pm 4.5$  mm for PSF, and  $13.8 \pm 3.9$  mm for CMF-PSF (all  $P < .05$ ). The CMF-PSF wall thickness was comparable to the thickness of the ED phase in the

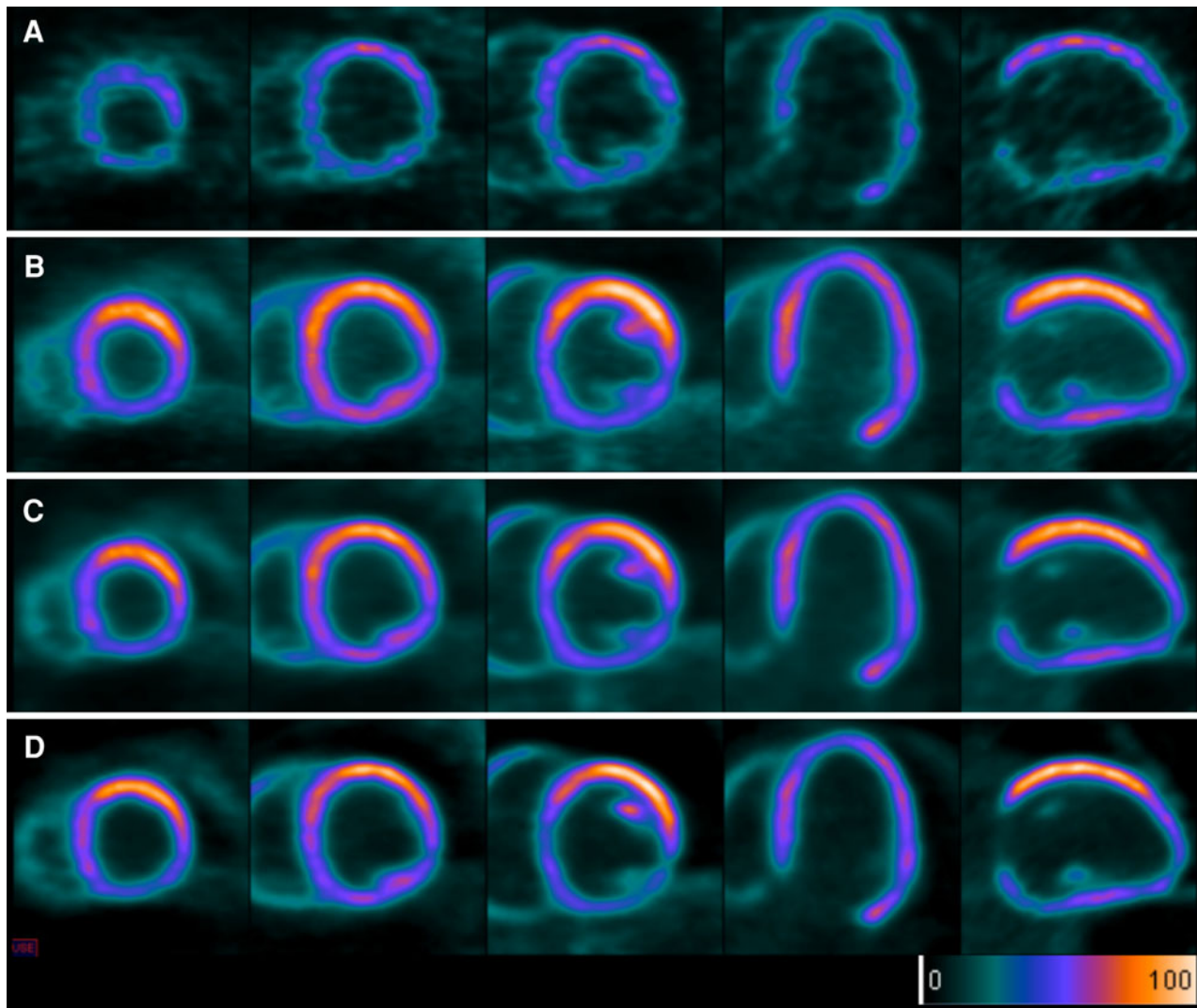


**Figure 2.** Example of an 89-year-old female patient ( $W = 87 \text{ kg}$  [193 lbs],  $\text{BMI} = 32.1$ ) referred for myocardium viability assessment. Image quality is improved with CMF-PSF (D) compared to end-diastole (ED) gated PSF (A), 2D-AWOSEM (B) and regular PSF (C). The wall thickness with CMF-PSF (D) is reduced compared to the summed static images and similar to the ED phase of the gated images but the noise is drastically decreased compared the gated dataset (A).

gated dataset reconstructed with PSF ( $13.3 \pm 3.3 \text{ mm}$ ,  $P = \text{NS}$ ). The results are summarized in Table 2. An example of improvements with CMF-PSF reconstruction in terms of visual image quality can be seen in Figure 2.

#### Myocardium to Blood Contrast and Contrast-to-Noise Ratio

The authors found that the myocardium to blood contrast was significantly increased with CMF processing. The average ratio of counts between the blood pool and the myocardium for 20 patients increased from  $3.5 \pm 1.4$  for 2D-AWOSEM,  $3.9 \pm 1.7$  for PSF,  $3.9 \pm 1.6$  for ED-gated PSF, to  $5.7 \pm 2.7$  for CMF-PSF

reconstructions (CMF vs all,  $P < .05$ ). Meanwhile, the CNR was also significantly increased with CMF or similar to summed static image. The CNR was increased by 30% compared to 2D-AWOSEM, and by 90% compared to ED-gated image reconstructed with PSF (both  $P < .05$ ), and was similar to PSF ( $29.1 \pm 18.3$  vs  $26.3 \pm 17.5$  for CMF-PSF,  $P = \text{NS}$ ). The full results can be found in Table 3. An example of the contrast and CNR comparison for all different reconstructions and processing is shown in Figure 2. Furthermore, the authors have found that as expected, the increase of contrast between the blood pool and the mean in each segment when CMF was used is significantly correlated to the amount of wall motion per segment (Figure 3).

**Table 2.** Myocardial wall thickness (in mm) measured on profiles taken at basal, mid, and apical levels from septal (sep) to lateral (lat) and from superior (sup) to inferior (inf)

Wall thickness (in mm)	Basal		Mid		Apical		Average
	Sep-to-lat	Sup-to-inf	Sep-to-lat	Sup-to-inf	Sep-to-lat	Sup-to-inf	
2D-AWOSEM	17.6 ± 4.6	19.0 ± 3.6	18.3 ± 5.4	19.4 ± 4.6	21.8 ± 8.4	17.0 ± 4.4	18.9 ± 5.2
PSF	16.5 ± 4.5	17.2 ± 3.5	15.8 ± 3.3	17.3 ± 4.7	18.1 ± 7.7	14.8 ± 3.1	16.6 ± 4.5
ED-Gated PSF	12.9 ± 3.8	12.8 ± 2.0	13.7 ± 2.4	13.8 ± 3.6	14.1 ± 4.4	12.7 ± 3.3	13.3 ± 3.3
CMF-PSF	13.0 ± 3.0	14.0 ± 3.6	13.7 ± 2.7	14.2 ± 4.6	14.8 ± 5.9	13.0 ± 4.0	13.8 ± 3.9

Results for 2D-AWOSEM, PSF, end-diastole (ED)-gated PSF and cardiac motion frozen (CMF)-PSF.  
All  $P < .05$  except ED-Gated HD-PET versus CMF-HD-PET where  $P = \text{NS}$ .

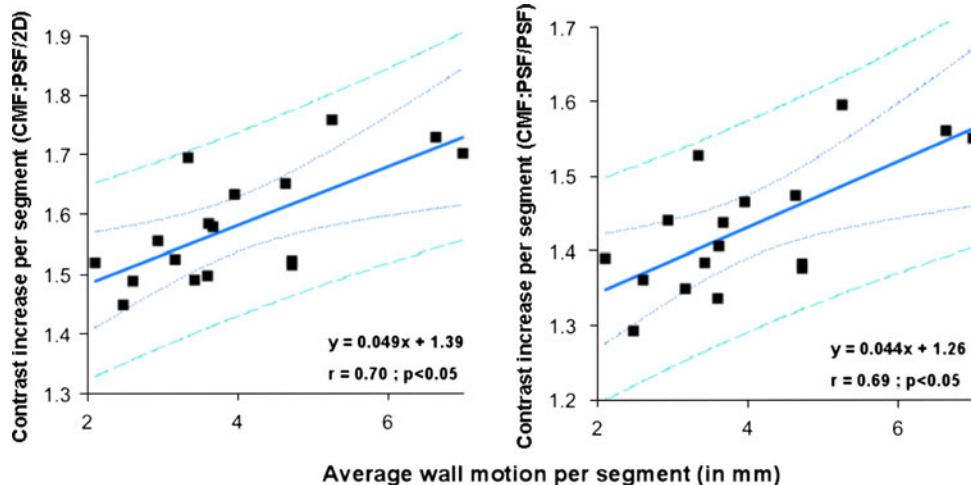


**Figure 3.** Segmental contrast increases with CMF against wall motion per segment. For each patient, the authors calculated the contrast between the blood pool and the mean value in each of the 17 segments. We then calculated the contrast increase for each segment with the use of Cardiac Motion Frozen technique and the authors plot the results against the segmental wall motion. The plots show the average over the 20 patients. This figure shows linear correlation between the segmental contrast increase with CMF, and the corresponding wall motion.

**Table 3.** Myocardial to blood contrast and contrast-to-noise (CNR) for 2D-AWOSEM, PSF, end-diastole (ED) gated PSF and cardiac motion frozen (CMF) PSF

	2D-AWOSEM	PSF	ED-Gated PSF	CMF-PSF
Contrast	3.5 ± 1.4	3.9 ± 1.7	3.9 ± 1.6	5.7 ± 2.7
CNR	21.0 ± 11.9	29.1 ± 18.3*	13.7 ± 8.8	26.3 ± 17.5

$P < .05$  for CMF-PSF versus other techniques except for the value marked \*.

### Contrast Between Defect and Maximum Uptake in Myocardium

In the 20 patients considered in this study, there were a total of 71 segments identified as abnormal by visual analysis. With CMF, the authors found a significant

change in the contrast between the average of the closest neighbors around the minimum in segments with defects and the average of the closest neighbors around the maximum of the myocardium. In these segments, the contrast increased from  $6.5 \pm 3.1$  for 2D-AWOSEM, and

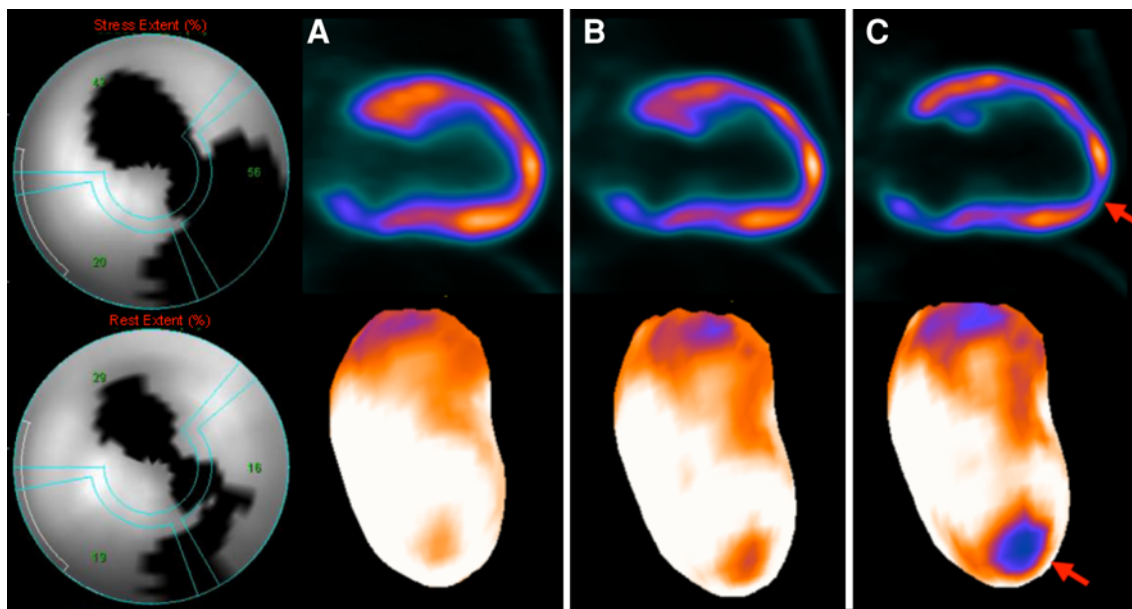


**Figure 4.** Example of an 84-year-old patient ( $W = 76$  kg [168 lbs],  $BMI = 27.1$ ) with a history of MI. The patient exhibits a non-reversible perfusion defect in the apical lateral region of the myocardium (Left SPECT perfusion images) as well as a moderate hypokinesis in the same region of the myocardium. The figure shows an example of increase of maximum LV counts to defect contrast with CMF-PSF (column C) in the horizontal long axis view (top row) and in the 3D rendering (bottom row). The apical lateral metabolic defect (red arrow) was not seen on 2D-AWOSEM (column A) and not clearly on PSF (column B) images.

from  $7.7 \pm 3.7$  for PSF to  $10.0 \pm 5.7$  for CMF-PSF reconstructions ( $P < .05$ ). An example illustrating the improved maximum LV counts to defect contrast is shown in Figure 4.

## DISCUSSION

“CMF” image processing technique compensates for the cardiac motion blur in the static images and has been shown to improve myocardial perfusion SPECT.<sup>3,10</sup> In this study, we have demonstrated that it further improves the technical cardiac image quality obtained with PSF reconstruction.

The measured myocardial wall thickness was significantly decreased with CMF-PSF ( $-27.0\%$  compared to 2D-AWOSEM and  $-16.9\%$  compared to PSF reconstruction alone). The average wall thickness ( $13.8 \pm 3.9$  mm) for the CMF-PSF reconstruction was comparable to the ED thickness (which has no cardiac motion) measured on gated PSF-reconstructed images ( $13.3 \pm 3.3$  mm) ( $P = \text{NS}$ ). Also, our wall thickness results are still larger than the average size in humans ( $10.3 \pm 1.2$  mm at ED) according to Kaul et al.<sup>11</sup>

The CNR for the CMF-PSF images was significantly increased compared to 2D-AWOSEM, but not compared to PSF reconstruction without CMF, for which the results were equivalent. However, the CNR

was significantly improved with CMF-PSF and compared to the ED phase of gated PSF reconstruction.

Increased contrast and equivalent CNR compared to static reconstructions, and wall thickness comparable to ED-gated images lead to a better image quality in general with CMF processing, which can easily be seen in the images. Furthermore, the authors have shown that the contrast between the defects, and a region of interest around the maximum of the myocardium was significantly increased with CMF. An example of a patient image with a metabolic defect, which is only clearly visible with CMF processing, and which is likely to exist based on the patient’s SPECT perfusion image findings is shown in Figure 4.

As expected, our cohort of patients has a relatively low EF. It is true that patients with low EF will have hypokinetic regions benefiting from smaller extent from the CMF technique. However, they often show both segments with preserved function and segments with impaired function. Since the CMF processing technique uses the wall motion as input, the segment-to-blood contrast is more increased for the segments with a preserved myocardial function than for the segments with an impaired function (as shown in Figure 3). In consequence, the contrast between the viable segments and unviable segments is increased with CMF (as shown by our results).

Because of the limited spatial resolution of PET, the partial volume effect leads to more counts/per pixel in the systole. The CMF technique has originally been developed for SPECT, which suffers from similar resolution limitations. CMF adds the counts from the majority of the cardiac cycle after spatial registration to the ED phase—as opposed to adding the counts in the cardiac cycle without any adjustments for motion. The CMF images are not only considered as diastolic images, but also as improved summed images. Therefore, CMF images of the dyskinetic myocardium will have similar counts as the simply summed image, which includes all phases (as it is performed in current clinical practice).

In this study, CMF was only applied to FDG viability studies. The authors did not have access to the raw perfusion data for those specific patients since most of them underwent SPECT perfusion imaging in a different facility. However, CMF processing has been shown previously to improve the image quality and the diagnostic in SPECT perfusion images in<sup>3,10</sup>. Therefore, for clinical applications, CMF technique should perhaps be used both for viability PET and perfusion SPECT when they are compared for viability assessment. This study was focused on a pilot application of CMF technique to high-resolution data demonstrating improved image quality. The improvement in quality should also be seen in the future in PET perfusion images using new tracer like flurpiridaz F18.<sup>12,13</sup> However, the authors did not have data in which both perfusion and viability were obtained by high resolution PET.

## Study Limitations

This study has several limitations. For instance, a gold standard did not exist for wall thickness of the myocardium. Also, there was no an external gold standard to confirm the presence or the absence of defects; however, in this study the authors focused on demonstrating the improvement in technical image quality. Whether the authors achieve results closer to the true tracer distribution, it remains to be further investigated. Our cohort of patients had a limited range of BMI, typical of our patient population. Our sample size was small (N = 20) and limited to viability studies; further studies with larger number of patients and PET perfusion images are warranted. CMF images were reconstructed with 16 gates only. Since 8-bin gating is often used, the effect of the temporal resolution with the 8-bin gated datasets may need to be evaluated. However, the initial validation study of CMF did test the difference between 8 and 16 gated datasets and the results were comparable.<sup>3</sup>

## CONCLUSIONS

Our study on <sup>18</sup>F-FDG viability studies showed that CMF processing increased myocardial-to-blood contrast and maximum LV counts to defect contrast while maintaining equivalent noise when compared to static summed images reconstructed with standard and modern reconstruction techniques incorporating resolution recovery. The significantly decreased myocardial wall thickness with CMF-PSF led to a better image quality in general.

## Acknowledgments

The authors want to thank Jimmy Fermin and Brandi N. Huber from Cedars-Sinai Medical Center for their help with the PET acquisition, and Heidi Gransar for her help with the statistical analysis.

## Open Access

This article is distributed under the terms of the Creative Commons Attribution Noncommercial License which permits any noncommercial use, distribution, and reproduction in any medium, provided the original author(s) and source are credited.

## References

- Panin VY, Kehren F, Michel C, Casey M. Fully 3-D PET reconstruction with system matrix derived from point source measurements. IEEE Trans Med Imaging 2006;25:907-21.
- Le Meunier L, Slomka P, Dey D, Ramesh A, Thomson L, Hayes S, et al. Enhanced definition PET for cardiac imaging. J Nucl Cardiol 2010;17:414-26.
- Slomka PJ, Nishina H, Berman DS, Kang X, Akincioglu C, Friedman JD, et al. “Motion-frozen” display and quantification of myocardial perfusion. J Nucl Med 2004;45:1128-34.
- Kudo T. Metabolic imaging using PET. Eur J Nucl Med Mol Imaging 2007;34:49-61.
- Jonsson C, Odh R, Schnell PO, Larsson SA. A comparison of the imaging properties of a 3-and 4-ring biograph PET scanner using a novel extended NEMA phantom. IEEE Nucl Sci Symp Conf Rec 2007;4:2865-7.
- Townsend D, Jakoby B, Long M, Carr C, Hubner K, Guglielmo C, et al. Performance and clinical workflow of a new combined PET/CT scanner. J Nucl Med 2007;48:437.
- Kadri D, Casey M, Conti M, Jakoby B, Lois C, Townsend D. Impact of time-of-flight on PET tumor detection. J Nucl Med 2009; 50:1315.
- Slomka P, Dobala S, Berman D, Gerlach J, Germano G, DiCarli M. Automated quantification and normal limits for myocardial perfusion stress/rest Rb-82 PET/CT. J Nucl Med 2009;50:1164.
- Cerdeira M, Weissman N, Dilsizian V, Jacobs A, Kaul S, Laskey W, et al. Standardized myocardial segmentation and nomenclature for tomographic imaging of the heart a statement for healthcare professionals from the Cardiac Imaging Committee of the Council on Clinical Cardiology of the American Heart Association. 2002, p. 539-42
- Suzuki Y, Slomka P, Wolak A, Ohba M, Suzuki S, De Yang L, et al. Motion-frozen myocardial perfusion SPECT improves detection of coronary artery disease in obese patients. J Nucl Med 2008;49:1075.

11. Kaul S, Wismer G, Brady T, Johnston D, Weyman A, Okada R, et al. Measurement of normal left heart dimensions using optimally oriented MR images. Am J Roentgenol 1986;146:75.
12. Yu M, Guaraldi M, Mistry M, Kagan M, McDonald J, Drew K, et al. BMS-747158-02: A novel PET myocardial perfusion imaging agent. J Nucl Cardiol 2007;14:789-98.
13. Le Meunier L, Slomka P, Ramesh A, Thomson L, Hayes S, Tamarappoo B, et al. Enhanced dual gated cardiac perfusion PET using a new F-18 imaging agent (BMS747158). J Nucl Med 2010;51:522.